Delay Equalization of Eight-Kilocycle Carrier Program Circuits

By C. H. DAGNALL and P. W. ROUNDS

This paper describes the equalization of delay in 8-kc program systems transmitted over broad-band carrier telephone facilities. Use is made of a condenser-plate potential analog which provides a ready method for blocking out the basic design and arriving at the final equalizer constants. Most of the equalization is accomplished at audio frequencies, and the remainder at carrier frequencies with quartz-crystal equalizers.

IN TRANSMITTING programs for radio broadcasting over the United States, an extensive network of wire circuits has been established by the Bell System. Most of the additions to this network since the war have employed a single-sideband carrier system[5] applicable to broad-band carrier facilities. The selection of a single sideband requires sharp frequency discrimination, and when this discrimination is achieved with minimum-phase structures, it is of necessity accompanied by delay distortion.[3]

In one or two carrier links, each including a transmitting and receiving terminal, the delay distortion is sufficiently small so that no deterioration in the program is noticeable. However, flexibility of maintenance and operation of an extensive program network requires that the network be built up of a large number of links in tandem. When this is done, the effects of delay distortion become quite conspicuous and equalization of the delay is necessary. Furthermore, if the equalization is to be satisfactory between any two points in the network, each link must be independently equalized.

Most of the delay distortion arises in the carrier-frequency band-pass filter which selects the lower sideband, the small remaining portion being contributed by the amplifiers and repeating coils. Figure 1 illustrates the unequalized delay in one terminal. Equalizers have been added to each terminal to make the phase characteristic approach linearity and so permit at least ten links to be operated in tandem without excessive distortion.

Theory of Design

The equalization of delay distortion is accomplished through the use of all-pass networks which, in their most general form,[2] may be constructed as a tandem set of lattice sections of the type shown in Fig. 2. An electrostatic analogy, developed during the late thirties,[4] has been found to be of great assistance in visualizing the performance of these networks and in indicating a rational method of design.

Considering the single section shown in Fig. 2 as the basic building block, the loss and phase may be expressed in the form

$$e^{A+jB} = \frac{(p + k_n - j\omega_n)(p + k_n + j\omega_n)}{(p - k_n - j\omega_n)(p - k_n + j\omega_n)} \tag{1}$$

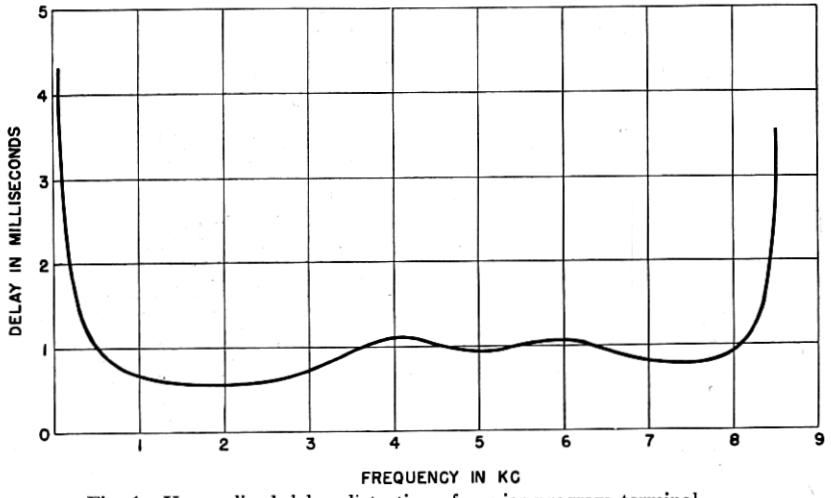

Fig. 1—Unequalized delay distortion of carrier program terminal.

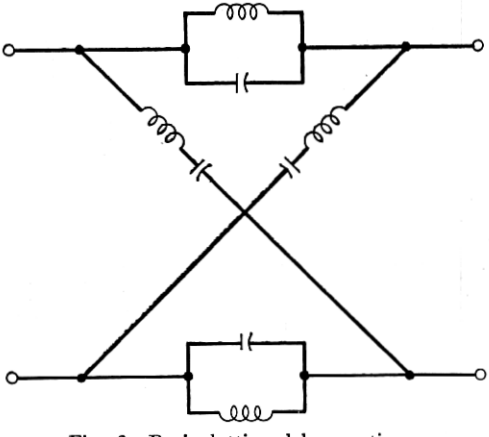

Fig. 2—Basic lattice delay section.

where

A = insertion loss in nepers
B = insertion phase in radians
p = $j\omega$
ω = frequency in radians per second
k_n, ω_n = real positive constants

An examination of equation (1) indicates that there are zeros at the two points:

$$p = -k_n + j\omega_n \text{, and } p = -k_n - j\omega_n$$

and poles at the two points

$$p = +k_n + j\omega_n \text{, and } p = +k_n - j\omega_n$$

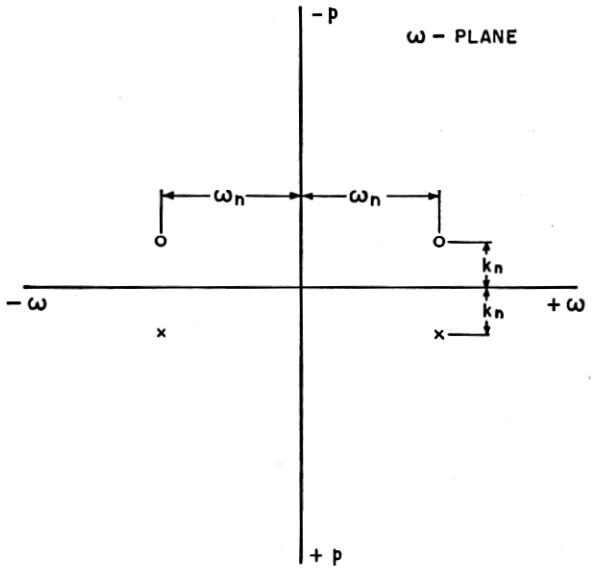

Fig. 3—Plot of zeros and poles of the network of Figure 2 on the complex-frequency plane.

The first zero in equation (1) contributes a delay (defined as the derivative of the phase with respect to frequency) of the form

$$T_1 = \frac{dB_1}{d\omega} = \frac{1}{k_n\left[1 + \frac{(\omega - \omega_n)^2}{(k_n)^2}\right]} \tag{2}$$

Similar expressions may be obtained for the other zeros and poles, the total delay of the section then being equal to the sum of the delays contributed by each zero and pole.

The four zeros and poles of equation (1) may be plotted on the complex-frequency plane as shown in Fig. 3, where the circles indicate zeros and the crosses poles. The four points are seen to be symmetrically disposed with respect to the origin. With reference to this figure, it will be noted that, since $\omega = -jp$, positive real values of p correspond to negative imaginary

values of ω and negative real values of p correspond to positive imaginary values of ω. The axes of Fig. 3 have been labelled accordingly.

It is at this point that the electrostatic analogy begins to come into play. Assume that an infinite wire filament, positively charged throughout its length, is run through the zero $p = -k_n + j\omega_n$ perpendicular to the plane of the paper and that a unit positive charge is placed at an arbitrary point, ω, along the real frequency axis. The component of the force normal to the ω axis exerted on the unit charge may be written in the form

$$F = \frac{1}{k_n \left[1 + \frac{(\omega - \omega_n)^2}{(k_n)^2} \right]} \tag{3}$$

When distances in equation (3) are identified with frequencies in equation (2), the two expressions are identical. A similar argument applies to the other zero, and also to the two poles provided that the filaments passing through the poles have charges of the opposite polarity. Thus we may say that the network of Fig. 2 will have a delay proportional to that component of the electric field intensity which is normal to the ω axis, when a positive filament passes through each zero and a negative filament through each pole. Fig. 4 indicates the character of the delay as a function of frequency. Parenthetically we may note that the component of the field intensity parallel to the ω axis is proportional to the derivative of the loss. Since this component is zero, the loss will be constant at all frequencies. In the case of the reactance networks with which we are dealing here, the loss is zero.

Although the usefulness of the electrostatic analogy lies principally in its application to more complex networks, several conclusions may be drawn from Fig. 4. The right-hand zero and pole, because of their symmetrical spacing and opposite charges, make equal contributions to the total delay. The same statement holds true for the left-hand zero and pole combination. As the zeros and poles approach the real-frequency axis, the delay peaks become sharper and higher because of the increased local field intensity. The figure also shows that the slope of the delay curve is zero at zero frequency and that, unless ω_n is large compared to k_n, the delay at zero frequency is of appreciable magnitude. These isolated facts will be exploited later in considering more complex networks.

Assume, now, a tandem series of sections of the type shown in Fig. 2, in which the zeros and poles are so selected that they are evenly spaced at intervals, a, along straight lines parallel to the real-frequency axis as shown in Fig. 5. It was pointed out by H. W. Bode[1] that the resulting field intensity may be approximated by distributing the total of the discrete charges on the plates of an equivalent condenser passing through the zeros and poles and extending a distance of $a/2$ beyond the extreme zeros and

poles. This approximation ignores the ripples caused by the granularity of the filament spacings, but it does permit the average delay to be determined in a particularly simple manner. The field intensity at any point, ω,

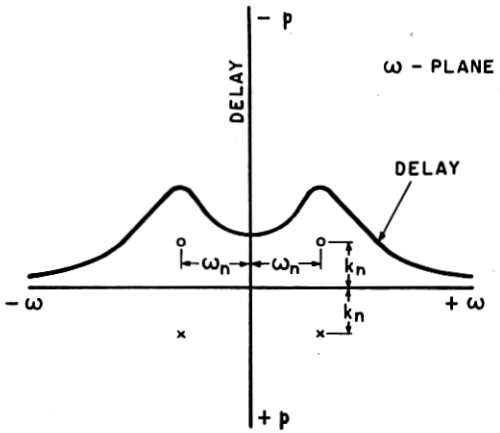

Fig. 4—Delay-frequency characteristic of the network of Fig. 2.

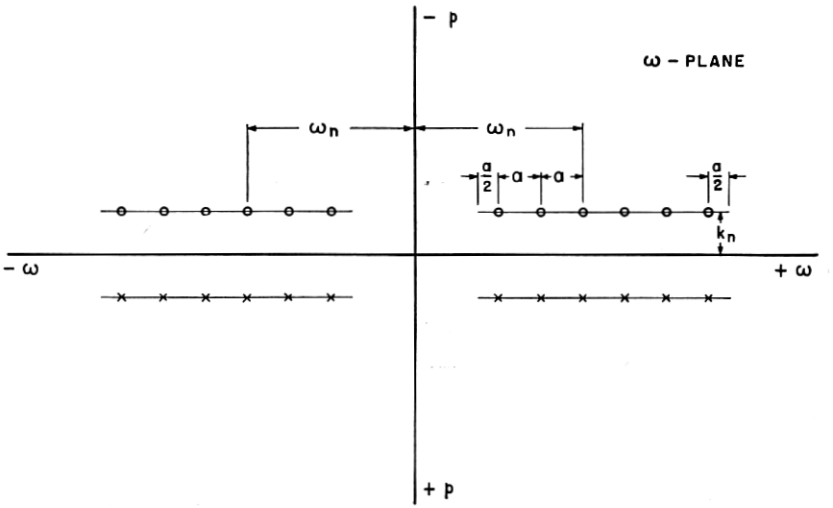

Fig. 5—Zeros and poles of a complex delay network based on the condenser-plate design.

resulting from the condenser charge is proportional to the angle subtended by the plates at that frequency. It is also proportional to the charge per unit length of plate or, in other words, to the density, $1/a$, of the filament spacings. The geometry is illustrated in Fig. 6, where $2(c + d)$ is the

angle subtended by the plates at the frequency ω. From this figure it may be seen that the field intensity in the region between the plates will have a fairly uniform value which falls off sharply as the edges are reached and becomes vanishingly small at frequencies remote from the plates.

Along with this simple determination of the average delay characteristic, D. F. Tuttle in an unpublished memorandum has derived expressions for the magnitude of the delay ripple. As shown in the appendix, the field

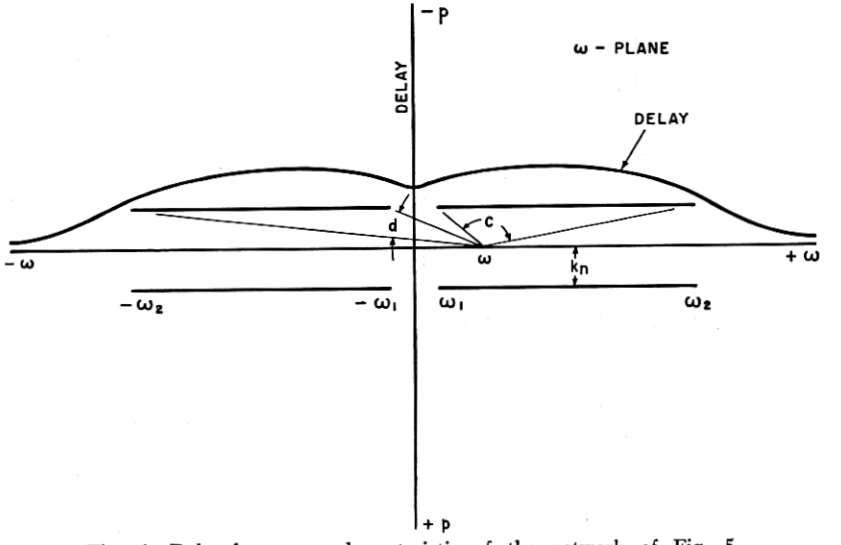

Fig. 6—Delay-frequency characteristic of the network of Fig. 5.

intensity or delay for an infinitely long set of charged filaments may be expressed in the form

$$T = \frac{2\pi}{a} \tanh \frac{2\pi k_n}{a} \left[1 - \left(\frac{\cos \frac{2\pi\omega}{a}}{\cosh \frac{2\pi k_n}{a}} \right) + \left(\frac{\cos \frac{2\pi\omega}{a}}{\cosh \frac{2\pi k_n}{a}} \right)^2 - \cdots \right] \tag{4}$$

For reasonably large values of $2\pi k_n/a$, this relation may be replaced by the approximate expression

$$T \approx T_0[1 - \delta \cos T_0\omega] \tag{5}$$

where $T_0 = 2\pi/a$ is the average delay and $\delta = 2e^{-T_0 k_n}$ is the percentage ripple about the average value. The ratio k_n/a may thus be determined from the percentage delay ripple in accordance with the formula

$$\frac{k_n}{a} = \frac{1}{2\pi} \log_e \frac{2}{\delta} \tag{6}$$

To equalize the low-frequency and high-frequency filter delay shown in Fig. 1, a condenser plate of the form shown in Fig. 6 might be visualized. Although the high-frequency delay approximates that desired, the low-frequency delay shows insufficient shaping to be complementary to the filter characteristic because of the contribution of the negative-frequency plates. By bringing the plates closer to the frequency axis, that is by decreasing the ratio k_n/ω_1, a sharper-breaking low-frequency characteristic could be obtained. However, to achieve a sufficiently small delay ripple, the spacing, a, as determined from equation (6) would then have to be decreased with the result that the number of sections would be correspondingly increased.

In attempting to reduce the total number of sections required, it was observed that a carrier-frequency delay equalizer would not be subject to

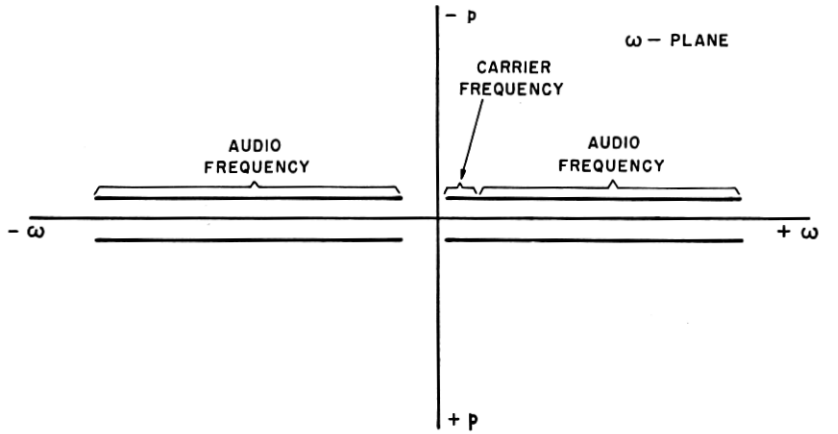

Fig. 7—Condenser-plate design for a combined carrier and audio-frequency delay equalizer.

the same low-frequency limitation, since the negative-frequency plates would be removed from the single-sideband signal by approximately twice the carrier frequency of 88 kc. However, since high-frequency delay sections are more expensive to construct than those operating at audio frequencies, a compromise is made in which the first few sections are built to operate at carrier frequencies and the remaining sections at audio frequencies. The equivalent condenser plates, referred to the audio-frequency signal, are shown in Fig. 7.

A condenser-plate design has thus been achieved which allows the low-frequency and high-frequency delay to be equalized at least approximately. Further modifications must be made in the design, particularly in the middle of the band, to shape the characteristic so that a more accurate complement of the filter delay may be obtained. The delay in a condenser-

plate design is directly proportional to the charge density along the plate. Up to now, this density has been assumed to be uniform. When the charge is located on discrete filaments, the restriction of uniform density is no longer necessary and it is possible to modify the delay characteristic as desired by changing the spacing of the filaments in inverse proportion to the desired change in delay.

The assumption of a flat plate is also useful in simplifying the analysis; in the actual design the equivalent plate is bowed out over the major portion of the frequency range to reduce the delay ripple. The final zeros and poles obtained are shown in Fig. 8, in which the carrier-frequency zeros and poles are plotted on an equivalent audio-frequency basis. A total of 29

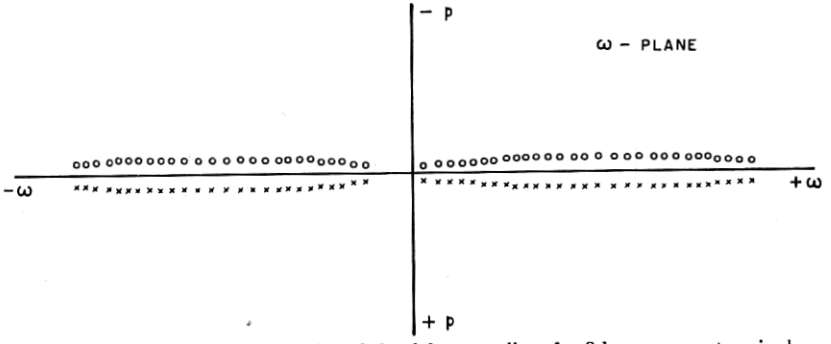

Fig. 8—Plot of the zeros and poles of the delay equalizer for 8-kc program terminals.

delay sections are required, of which three are assigned to the carrier-frequency equalizer and 26 to the audio-frequency equalizer.

Audio-Frequency Equalizer

To complete the design of the audio-frequency equalizer some means must be found for absorbing the effects of dissipation in the coils and condensers so that the final dissipative network will exhibit the theoretical non-dissipative performance plus a loss which is constant with frequency. It can be shown that a non-dissipative all-pass section plus a flat-loss pad can be replaced with a dissipative all-pass section (of modified constants) in tandem with a minimum-phase loss equalizer as in Fig. 9. It would be uneconomical to associate a loss equalizer with every phase section; and it is in fact unnecessary, since any minimum-phase device accomplishing the same result will exhibit the same performance.[3] The problem is then reduced to equalizing the loss of the network composed of dissipative delay sections.

The dissipative loss of these sections may be determined from the approximate relation

$$\text{Dissipative Loss in nepers} \approx \frac{1}{2}\left(\frac{R}{L} + \frac{G}{C}\right) T \tag{7}$$

where

$\frac{R}{L}$ = resistance-inductance ratio of coils in ohms per henry

$\frac{G}{C}$ = conductance-capacitance ratio of condensers in micromhos per microfarad

T = delay of network in seconds

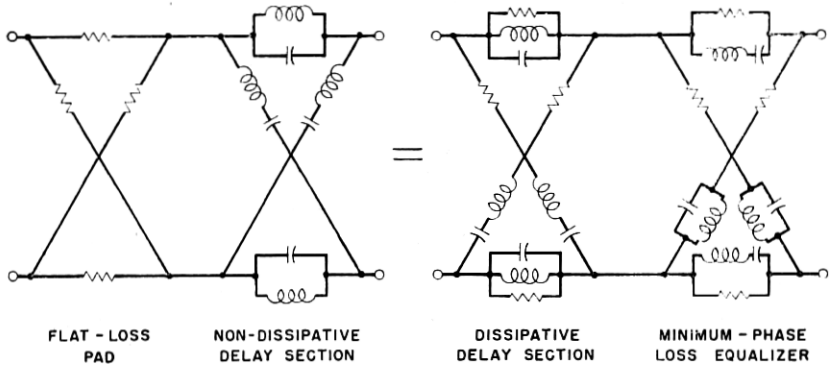

Fig. 9—Four-terminal equivalence showing the method of absorbing the effects of dissipation in the audio-frequency equalizer sections.

This expression indicates that, when the quantity $(R/L + G/C)$ is nearly constant with frequency, the shape of the loss characteristic will be generally similar to that of the delay characteristic. The ripples in the delay characteristic have been made sufficiently small so that the corresponding loss ripples may be ignored and only the general trend considered. A schematic of the resulting equalizer is shown in Fig. 10. The attenuation equalizer sections, in tandem with the delay sections, produce a loss characteristic complementary to that of the band filter over the 8000-cycle program range. Resistors have been added to the crossarms of each lattice delay section to allow the dissipative losses to be adjusted to the nominal values assumed in the design. For manufacturing convenience, the sections are assembled in seven separate containers which are mounted on an $8\frac{3}{4}$ inch by 19 inch relay-rack panel as illustrated in Fig. 11.

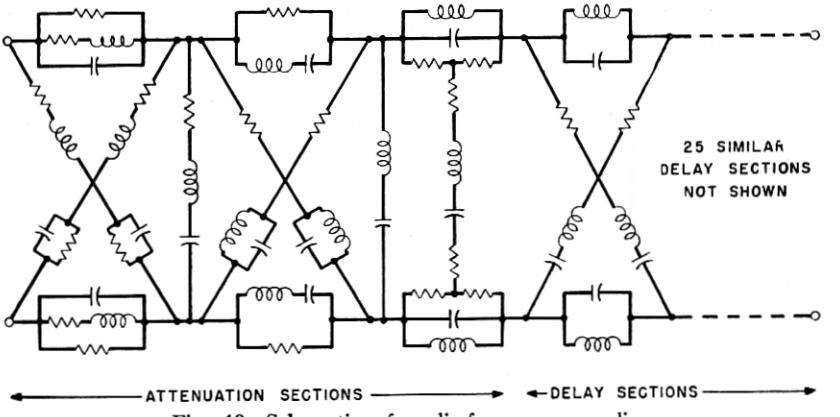

Fig. 10—Schematic of audio-frequency equalizer.

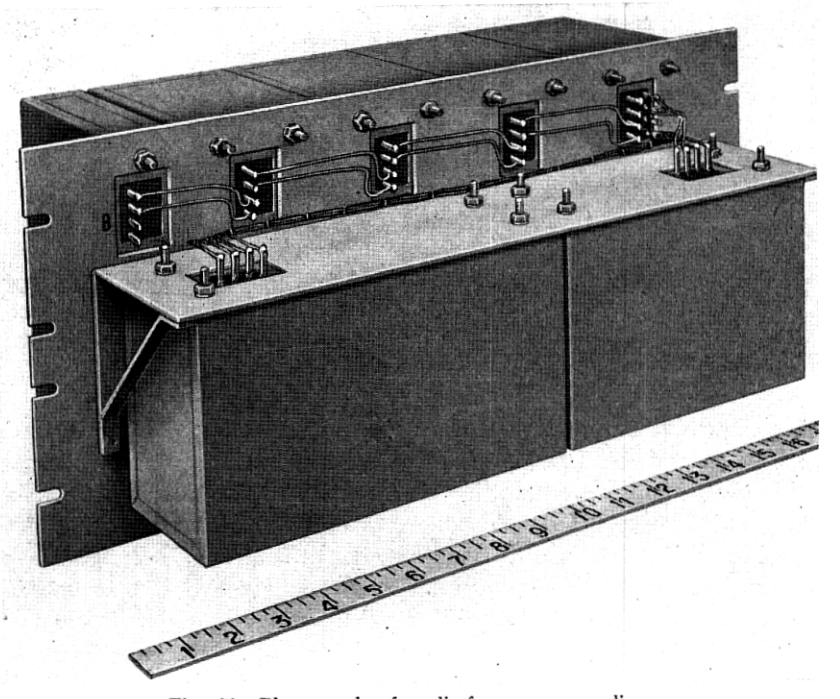

Fig. 11—Photograph of audio-frequency equalizer.

Carrier-Frequency Equalizer

The critical frequencies of the carrier-frequency equalizer are located at 318, 610 and 890 cycles on an audio basis. Since the carrier is at 88 kc

and the lower sideband is transmitted, the corresponding carrier frequencies are 87682, 87390 and 87110 cycles, respectively.

The required change of phase per cycle is the same as at audio frequencies, but the percentage rate of change is eleven times that of the audio-frequency sections operating at 8000 cycles. This requires that the arms of the sections have proportionately stiffer reactances, higher Q's, and greater tem-

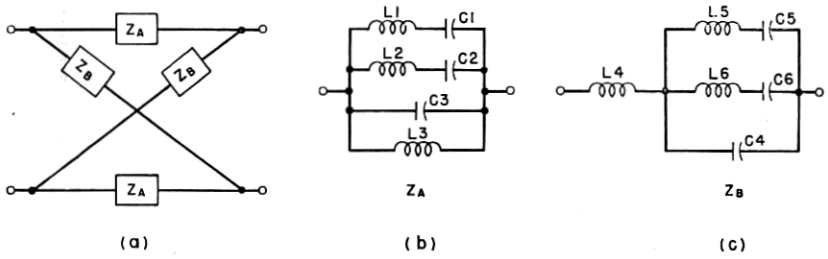

Fig. 12—Schematic of the lattice equivalent of three tandem sections of the type shown in Fig. 2.

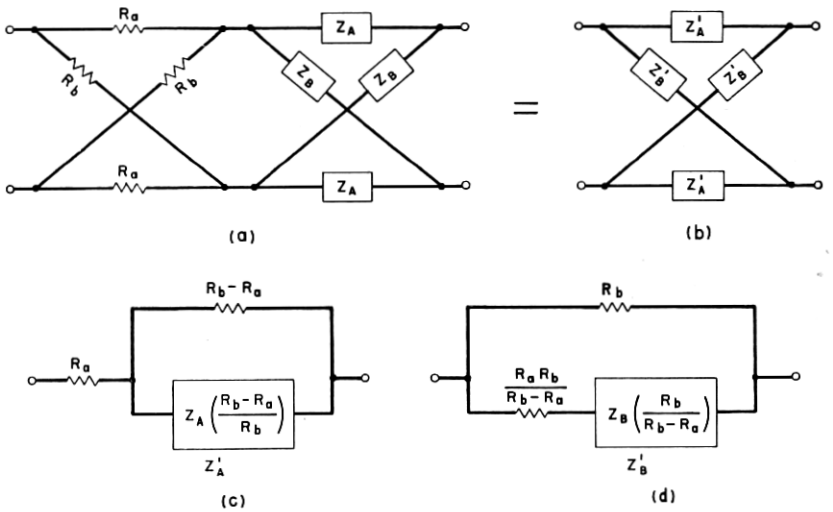

Fig. 13—Four-terminal equivalence showing the method of absorbing the effects of dissipation in the carrier-frequency equalizer.

perature stability. The only available elements meeting such requirements are piezo-electric crystals.

The approximate equivalent electrical circuit of a crystal is a capacitance in parallel with a series combination of an inductance and capacitance, and is not adaptable to the section of Fig. 2. However, when three such sections in tandem are combined into a single lattice, the configuration of

Fig. 12 is obtained. The stiffness of the reactances of arms Z_A and Z_B depends principally on the branches numbered 1, 2, 5 and 6. Each of these branches may be combined with a portion of C_3 or C_4 and replaced with a crystal.

One other restriction must be overcome before crystals can be used. Inductances L_1 and L_2 are in the order of 0.7 henry while L_5 and L_6 are in the order of 5000 henries, both inductance values being impractical for crystals. Two three-winding repeating coils are used to transform these inductances to values that may be provided by crystals. The two balanced windings of one repeating coil replace arms Z_B of Fig. 12(a), the third winding being connected to a reactance arm of the form of Fig. 12(c).

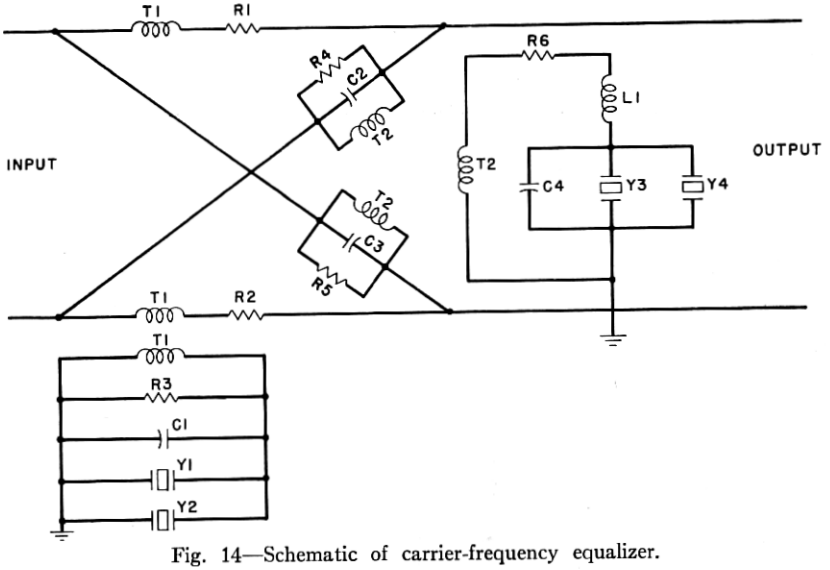

Fig. 14—Schematic of carrier-frequency equalizer.

The other repeating coil is similarly used for arms Z_A, the inductance L_3 being provided by the repeating coil. The repeating coils unavoidably introduce parasitic inductances, a small one in series with Z_A and a larger one in parallel with Z_B, the effects of which are made negligible by the addition of a capacitance in parallel with Z_B.

Dissipation in the elements of the carrier-frequency equalizer is taken into account by making use of the equivalence of Fig. 13, in which (a) represents the non-dissipative equalizer in tandem with a pad and (b) a structure similar to the non-dissipative structure but with resistances added to its arms, as shown by (c) and (d). The dissipation in each coil, condenser or crystal can be associated to a close degree of approximation with

one of these resistances. Physical resistances are added to compensate for deficiencies in dissipation. The loss of the pad is made large enough to allow for manufacturing deviations.

The complete schematic is shown in Fig. 14, and the equalizer with the shield removed in Fig. 15. Below the panel in Fig. 15, from left to right are arranged the retardation coil L1, adjusting condensers C1 and C4, the

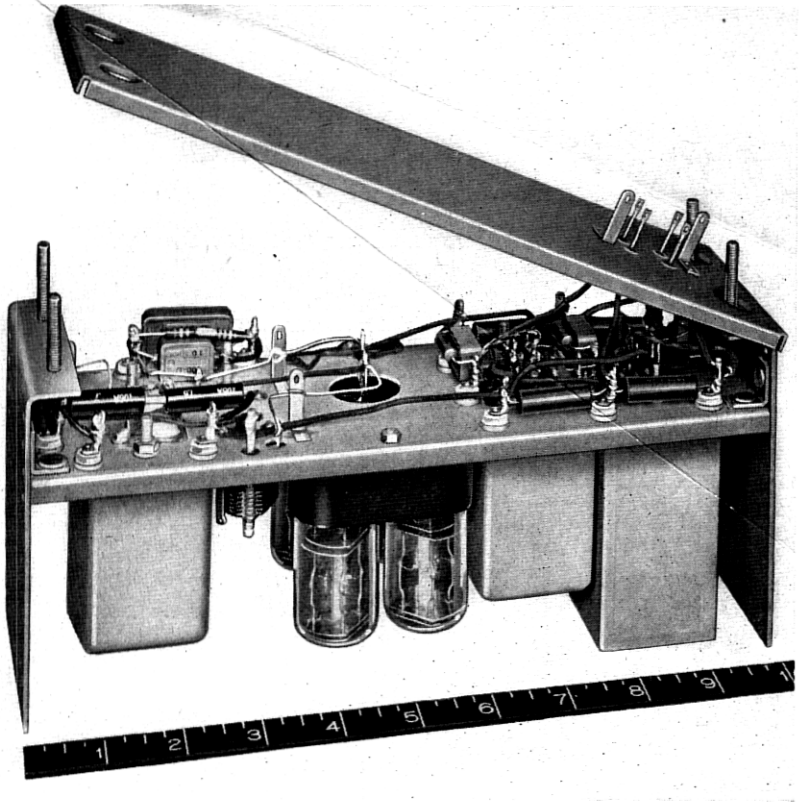

Fig. 15—Photograph of carrier-frequency equalizer.

crystals Y1 to Y4, inclusive, and the repeating coils T1 and T2. The fixed condensers and resistances are mounted above the panel.

Results

Curves *A* and *B* in Fig. 16 show the delay-frequency characteristics of the audio-frequency equalizer and the carrier-frequency equalizer, respectively. Curve *C* shows the equalized delay of one terminal, which is the sum of the delays of the equalizers added to the unequalized delay of Fig. 1.

Listening tests over ten carrier links in tandem indicate that the design objectives are sound and that a satisfactory reduction in delay distortion has been achieved.

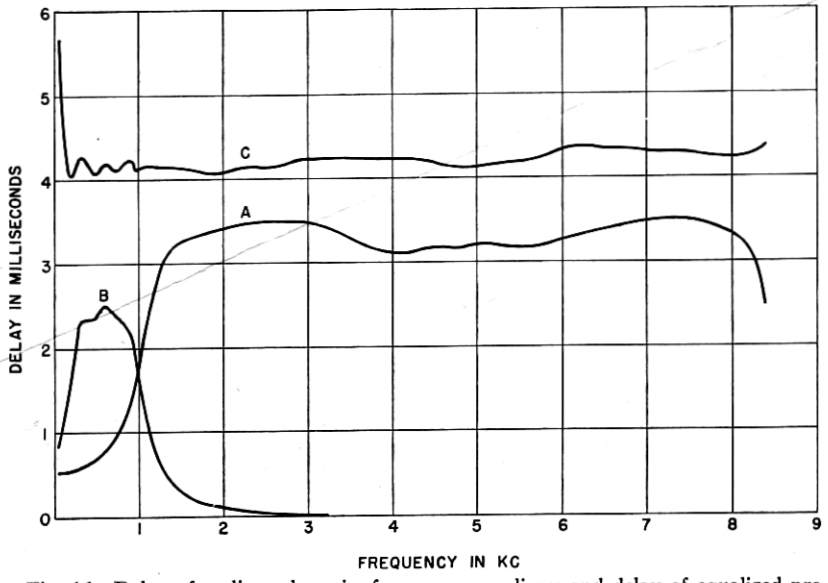

Fig. 16—Delay of audio and carrier-frequency equalizers and delay of equalized program terminal.

APPENDIX

For an infinitely long set of charged filaments of the type shown in Fig. 3 and located at $\omega = a/2,\ 3a/2,\ 5a/2$, etc., the insertion loss and phase may be expressed by the infinite-product expansion of equation (1),

$$e^{A+jB} = \prod_{n=1}^{\infty} \frac{[p + k_n - j(n - \tfrac{1}{2})a][p + k_n + j(n - \tfrac{1}{2})a]}{[p - k_n - j(n - \tfrac{1}{2})a][p - k_n + j(n - \tfrac{1}{2})a]}$$

$$= \prod_{n=1}^{\infty} \frac{1 - \left[\dfrac{i2(p + k_n)\pi/a}{(2n - 1)\pi}\right]^2}{1 - \left[\dfrac{i2(p - k_n)\pi/a}{(2n - 1)\pi}\right]^2} \tag{8}$$

Expression (8) is a standard form of product expansion and may be written

$$e^{A+jB} = \frac{\cos j(p + k_n)\pi/a}{\cos j(p - k_n)\pi/a} \tag{9}$$

or

$$A + jB = \log \cos j(p + k_n)\pi/a - \log \cos j(p - k_n)\pi/a \tag{10}$$

Substituting $j\omega$ for p and differentiating with respect to ω, we obtain

$$\frac{dA}{d\omega} + j\frac{dB}{d\omega} = j\frac{2\pi}{a}\frac{\sinh 2\pi k_n/a}{\cosh 2\pi k_n/a + \cos 2\pi\omega/a} \tag{11}$$

from which $dA/d\omega$ is zero. Equation (11) may be written

$$\frac{dB}{d\omega} = \frac{2\pi}{a}(\tanh 2\pi k_n/a)\left(\frac{1}{1 + \dfrac{\cos 2\pi\omega/a}{\cosh 2\pi k_n/a}}\right) \tag{12}$$

which, when expanded, gives equation (4).

References

1. "Wave Transmission Network," H. W. Bode, *United States patent* 2,342, 638.
2. "Network Analysis and Feedback Amplifier Design" (book) Chapter 11, H. W. Bode, D. Van Nostrand Co., Inc., New York, N. Y., 1945.
3. Reference 2, Chapter 14.
4. "Network Theory Comes of Age," R. L. Dietzold, *Electrical Engineering*, Volume 67, Number 9, September 1948, page 898.
5. "A Carrier System for 8000-cycle Program Transmission," R. A. Leconte, D. B. Penick, C. W. Schramm, A. J. Wier. A companion paper. This issue of *BSTJ*.
6. "Band Pass Filter, Band Elimination Filter and Phase Simulating Network for Carrier Program Systems," F. S. Farkas, F. J. Hallenbeck, F. E. Stehlik. A companion paper. This issue of *BSTJ*.